RESEARCH ARTICLE

Investigation of the Performance of Plugging Braking System as a Hill Descent Control (HDC) for Electric-Powered Wheelchair

P.M. Heerwan[1,2]*, M. A. Shahrom[1], M.I. Ishak[1], H. Kato[3], T. Narita[3]

[1]Faculty of Mechanical and Automotive Engineering Technology, Universiti Malaysia Pahang Al-Sultan Abdullah, Pekan, Malaysia
[2]Automotive Engineering Center, Universiti Malaysia Pahang Al-Sultan Abdullah, 26600, Malaysia
[3]Department of Mechanical System Engineering, Tokai University, 259-1207, Japan

ABSTRACT - Recently, a study on Electric Powered Wheelchairs (EPWs) has become significant because they can enhance the mobility of individuals with disabilities. One of the issues on EPW is during descending on a slope because it is difficult to control the speed and prevent it from slipping. Moreover, the manual braking system is frequently used for speed control by pressing the brake lever. The complexity of the task increases significantly when dealing with elderly or paralyzed users with physical limitations. Consequently, the risk of collisions and injuries is elevated. This research seeks to develop a hill descent control (HDC) system for an EPW to address these challenges. By implementing HDC into EPW, the EPW's speed can be controlled, thus increasing the safety of the EPW while descending on the slope. In this study, the plugging brake system is introduced as a hill descent control (HDC) mechanism to inhibit the acceleration of the EPW and ensure it maintains a constant speed during downhill descents. The plugging voltage will be controlled based on the desired speed of 0.6 m/s. To maintain the speed of the EPW, the PID control is used as a control strategy for HDC. The simulation work in Matlab Simulink has analyzed the performance of the plugging brake system with HDC. The results obtained from the simulation reveal that, despite starting with a high initial braking speed of 2.5 m/s, the Electric Powered Wheelchair (EPW) can consistently maintain its velocity at the desired target value of v_d = 0.6 m/s during the descent on the slope. Furthermore, the amplitude response for the PID control shows the settling time is 2.3 s, and the steady-state error is ±0.05. Based on the simulation results, it can be approved that the proposed HDC in the plugging brake system can prevent the EPW from accelerating while descending on the slope and improve the safety of the EPW.

1.0   INTRODUCTION

In general, the wheelchair can be divided into two categories, manual wheelchair and electric-powered wheelchair (EPW) [1]. Due to the advantages of EPW such as ease the users' mobility, the demand for EPW is increased. The Electric Powered Wheelchair (EPW) utilizes an electric motor within its drive system. It offers numerous benefits, such as compact size with potent output, precise torque control, and the capacity to generate electrical braking torque, namely regenerative braking [2].

Although EPW has several advantages, the main concern while using EPW is during descending on the slopes. The possibility of the EPW accelerating and skidding increases significantly when the inclination of the slope is high [3]. In Malaysia, the height of the slope is set by Malaysia Standard (MS-1184) which the slope must be lower than 1:12 or 4.8 degrees[4]. However, some of the buildings do not follow the Malaysia Standard requirement and can cause trouble for wheelchair users.

On the other hand, most EPWs are equipped with a mechanical braking system where the friction between the brake pad and wheel is generated when the user presses the brake pedal [5]. The problem with the mechanical brake system is that the braking force depends on the users' force[6]. People with disabilities and the elderly find it challenging to control themselves because descending a slope requires a significant amount of energy to stop or maintain speed [7].

By implementing the electrical braking control in the EPW, the active safety system can be enhanced in the EPW. During braking, the electric motor will generate the back electromotive force (EMF) [8]. As a result, the generated current from the back EMF will flow from the electric motor to the battery. The direction of this current is opposite to the rotational speed of the motor. Therefore, the braking torque is produced and consequently will reduce the speed of the motor. The back EMF represents an electrical braking torque, and it can be classified into three distinct types: regenerative, dynamic, and plugging. [9].

Dynamic braking involves the force of back-EMF current through the utilization of internal electronic resistors. Concurrently, the current, denoted as i_{emf}, is dissipated within the motor coil's internal resistance [10]. In DC motor applications, dynamic braking can be designed by shortening the motor terminals. The DC motor will stop rotating

immediately when the motor terminal is shortened. However, this will cause all the heat energy to dissipate in the motor[11]. A cooling system is needed for this method.

Researchers in [12] use dynamic braking to improve the safety features of the EPW during descending on the slope. They proposed a dynamic braking system based on a minimum acceleration during descending on the slope. By using a resistor, while dynamic braking is activating, the braking torque can stop the EPW in a safe region. Furthermore, the experimental result shows that the EPW's speed is the same as the desired speed when descending on the slope with a 6-degree inclination.

Due to the poor energy management of the dynamic braking, it is unsuitable for electrical transportation such as cars and EPW. Thus, the application of regenerative braking to electrical-based transportation becomes more practical. Energy generated by the motor can be captured by regenerative braking, thus enhancing the vehicle's dynamic movement [13]. In addition, the regenerative braking system can also increase the vehicle's traveling distance by harvesting electrical energy [14]. Theoretically, to execute regenerative braking, the back-EMF needs to exceed the supply voltage, causing the current i_{emf} to flow in the opposite direction to the current supplied by the voltage source [15].

The primary issue with the regenerative braking system arises when the generated back-EMF is less than the terminal voltage. Under such circumstances, the battery remains uncharged, and there is an absence of electrical braking generation. To enhance the back-EMF capacity, a control strategy utilizing the cascade bi-directional buck-boost converter was suggested by researchers in [16]. The function of a bi-directional buck-boost converter is to transfer the energy stored in the battery to the electric motor for driving mode conditions and reuse the energy from the back electromotive force (EMF) to charge the battery during braking conditions. Implementing the bi-directional buck-boost converter can store more energy in the battery when a vehicle is braking at a low speed. Moreover, the average power stored in the battery is enhanced by a factor of 2.5, leading to an improvement in the stopping time. The bi-directional buck-boost converter transfers the energy stored in the battery to power the electric motor during drive mode scenarios. It generates energy from the back electromotive force (EMF) to recharge the battery during braking situations. Incorporating the bi-directional buck-boost converter allows for greater energy storage in the battery when a vehicle is decelerating at a lower speed. Furthermore, this results in an enhancement of 2.5 in the average power stored in the battery, ultimately improving the braking time.

Although a bi-directional buck-boost converter can increase the back-EMF during regenerative braking activation, it is unsuitable for applying at the EPW since it needs an additional component that can increase the total load and cost of the EPW. Hence, the plugging braking system which uses the counter-current braking concept is more practical for the EPW. When plugging braking is engaged, the voltage supplied by the battery will switch direction, aligning with the back EMF, thereby compelling the armature current to flow in the reverse direction [17]. Consequently, the electrical braking torque will be generated and slow down the vehicle.

A plugging braking system for electric vehicles (EV) has been developed by [18] in the Matlab Simulink. The DC motor drive is fed by a bi-directional DC-DC converter in their study. The simulation results indicate that plugging brakes can safely bring the vehicle to a complete stop from an initial speed of 120 rad/sec, reducing it to 0 rad/sec. These findings indicate that the plugging brake is comparable to the hydraulic brake and can be an alternative brake system for electrical motor-based transportation.

Besides stopping the vehicle, a plugging braking system can also improve the vehicle's stability. A study by [17] shows that a plugging braking system can prevent the vehicle from skidding by controlling the slip ratio during emergency braking. However, inappropriate control of the braking counter current can cause the rotor bar of the motor to be broken. Thus, the traction and braking performance of the motor will be affected [19].

By using sensors and compiling the control algorithms in the electric motor, Hill Descent Control (HDC) can be implemented in the electric wheelchair. HDC can help reduce the risk of uncontrolled acceleration while descending the slope. The research on HDC for EPW has been developed by [20] to assist in navigating down the slopes. The step-up chopper circuit is linked in series with two motors to regulate the Electric Powered Wheelchair's (EPW) speed when navigating downhill. Employing the Minimum Jerk Model, the tire's speed is managed by adjusting the variable duty ratio. The experimental result shows that the proposed method can minimize errors between desired and actual speeds. Guo-Zhu et al. introduced a hybrid braking system (HDC) that combines regenerative and mechanical braking. The outcome demonstrates the desired speed is attained and sustained while descending the slope. In addition, the braking energy can be captured more from the regenerative braking system. Although HDC can improve the stability of EPW, the relation between wheel speed and HDC needs to be analyzed.

To improve the safety system and prevent the EPW from skidding while descending on the slope, plugging braking is a suitable system due to its advantage in providing the counter current to generate the braking torque. In addition, the counter-current can be controlled by the HDC system to maintain the speed of the EPW while descending on the slope. In this paper, plugging braking with HDC is proposed to improve the safety system of the EPW. In Matlab Simulink, the plugging braking system integrated with HDC was developed to assess the efficiency of the suggested control approach.

2.0   NUMERICAL ANALYSIS

The performance analysis of the plugging brake system with hill descent control is performed in the MATLAB Simulink. Figure 1 shows an instrumented electric-powered wheelchair (EPW) used as a reference to develop the EPW modeling in the simulation. This EPW consists of two in-wheel brushless DC motors to drive the EPW with a power supply of a 24V battery. Table 1 shows the specifications of the instrumented EPW. The hardware at the instrumented EPW consists of sensors, motors, batteries, and microprocessors.
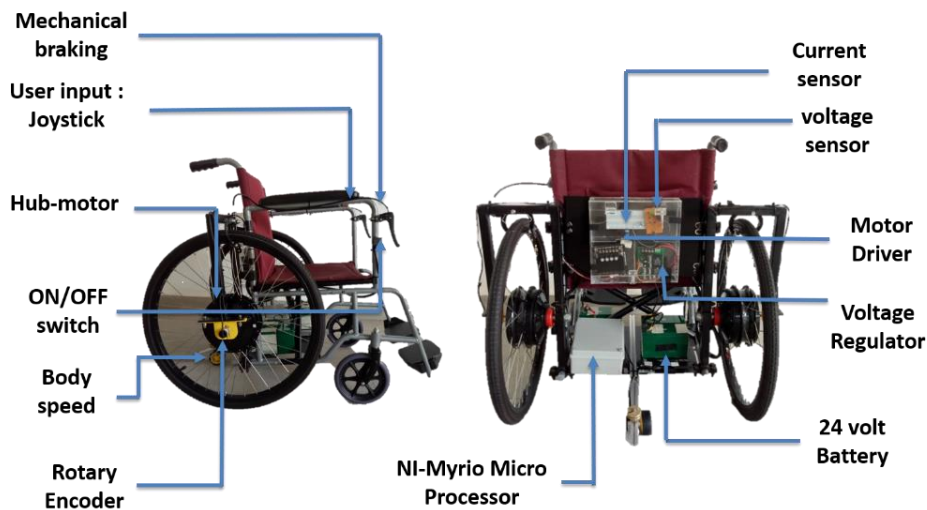
Figure 1. Instrumented electric-powered wheelchair

Table 1. Electric Powered Wheelchair (EPW) Specification

Feature	Specification
Motor type	In-wheel Brushless DC
Top speed (m/s)	2.7
Operating voltage (Volt)	12~36

2.1   Brushless DC (BLDC) Motor Modelling

This investigation's initial phase involves deriving an equation of the brushless DC (BLDC) motor intended for use in the Electric Powered Wheelchair (EPW). Figure 2 illustrates the BLDC motor's constituent parts, wherein the motor is represented with a single coil described by its inductance (L) resulting from the windings and resistance (R) attributed to conductor losses.
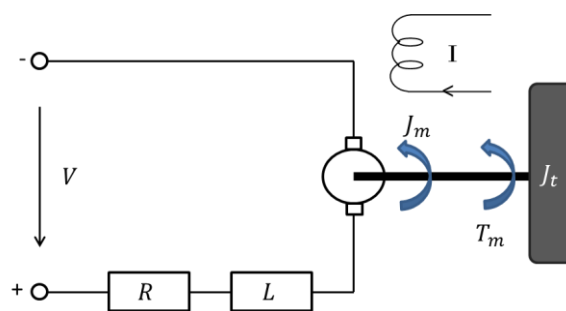

Figure 2. Electrical components of BLDC

Based on Figure 2, the equation of the BLDC motor can be derived as in Eq. 1:

$$\sum p(t)_{in} = \sum p(t)_{out} \tag{1}$$

where the power input $p(t)_{in}$ from the battery is the same as the power output $p(t)_{out}$. When the battery is connected to the BLDC motor, the electrical power to the power is iV, where i is the current and V is the voltage. The electrical energy will be converted into mechanical power, denoted as $\tau\omega$, with τ representing torque and ω signifying the rotational speed of the output shaft. Besides transforming to mechanical power, due to the resistance, R and inductance, L, the power input also will be transformed to the heat, i^2R. Furthermore, the inductance inside of the motor also can store the energy, motor also will store energy, $1/2(Li^2)$ in the inductor's magnetic field, and the time rate of change of this is $Li(di/dt)$. By combining all the input and output of the BLDC motor, Equation 1 can be rewritten as:

$$iV = i^2R + Li\frac{di}{dt} + \tau\omega \tag{2}$$

From Equation (2), by dividing the current at both sides, the relation of the input voltage from the battery to the BLDC motor output can be derived as follows:

$$V(t) = i(t)R + L\frac{di(t)}{dt} + \frac{\tau}{i(t)}\omega(t) \tag{3}$$

The ratio τ/i is a constant and also known as torque constant, k_t, and the SI units of k_t is Nm/A. Among the motor's key characteristics, the torque constant holds significant importance. By substituting τ/i into k_t in Equation (3), the BLDC motor model can be expressed as:

$$V(t) = i(t)R + L\frac{di(t)}{dt} + k_t\omega(t) \tag{4}$$

In Equation 4, the term $k_t\omega$, is recognized as the back electromotive force (back-EMF). It is also referred as "back-voltage".

2.2   Dynamic modeling of EPW

In Figure 3, the free-body diagram of the Electric-Powered Wheelchair (EPW) illustrates all the forces when descending on a slope. The gravitational force, represented as $mg\sin\emptyset$ along the longitudinal axis, resulting in the generation of gravitational torque T_g, which initiates the EPW's downward motion.
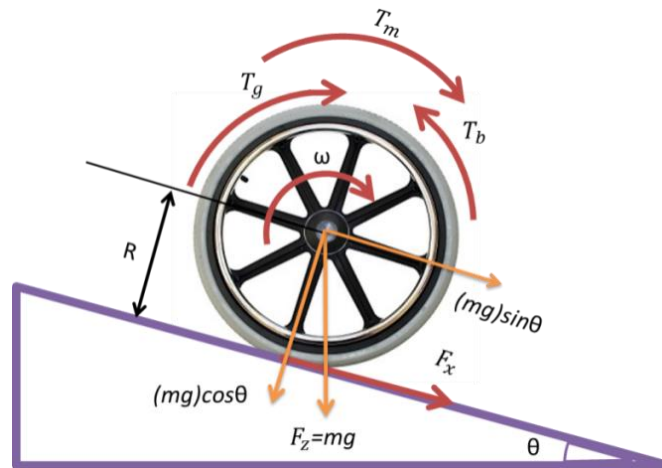

Figure 3. Forces acting on the EPW while descending on the slope

Based on the free body diagram in Figure 3, the wheel angular acceleration, $d\omega/dt$ can be determined by using Equation (5) as follows:

$$\frac{d\omega(t)}{dt} = \frac{T_m(t) + T_g(t) - T_L(t) - T_b(t) - B\omega(t)}{J} \tag{5}$$

where,

$$T_L = T_{int}(t) + T_f(t)$$

$$J = J_m + J_t$$

where T_m is the input torque of the motor, T_L is the load torque that consists of the initial torque in the motor, T_{int} and frictional torque, T_f. B and ω are bearing constant and rotational speed respectively. J is the moment of inertia, which is the sum of the motor's inertia, J_m and tire moment of inertia, J_t, and T_b is the braking torque.

Then, Equation 5 can be expended as Equation 6. The input torque motor, T_m is the product of the current, I and torque constant, k_t of the BLDC motor, while the gravitational torque, T_g is the product of the weight force at the longitudinal axis and tire radius, R_t. Simultaneously, the resistance torque, referred to as the friction torque T_F, is calculated as the product of the longitudinal friction F_x and the tire radius R_t:

$$\frac{d\omega(t)}{dt} = \frac{K_tI(t) + m_g\sin\theta R_t(t) - [T_{int}(t) + F_x(t)R_t] - T_b(t) - B\omega(t)}{J_m + J_t} \tag{6}$$

The braking torque, T_b that will be used in the simulation is the plugging braking. The BLDC motor will produce a back EMF that produces current while descending on the slope. To activate plugging braking, the armature voltage polarity will be reversed. As a result, the current direction will be altered, opposing the current carried by the back EMF voltage.

2.3   Dynamic Equation of Motion of EPW

Figure 4 shows the forces acting on the EPW at the longitudinal axis. In the simulation, the mass at the left and right tires is assumed to be distributed equivalently. Since EPW is moving at a low speed and not turning to the left and right, the lateral, yawing, pitch, and roll motions are neglected in the simulation analysis. Based on the Newton's Second Law, the equation of motion in the longitudinal axis is expressed as follows:

$$\sum F_x = m_{EPW} \dot{u}_x \tag{7}$$

where m_{EPW} is the mass of EPW, and $\dot{U}_x$ is the longitudinal acceleration. By integrating the $\dot{U}_x$, the longitudinal velocity, U_x can be obtained.
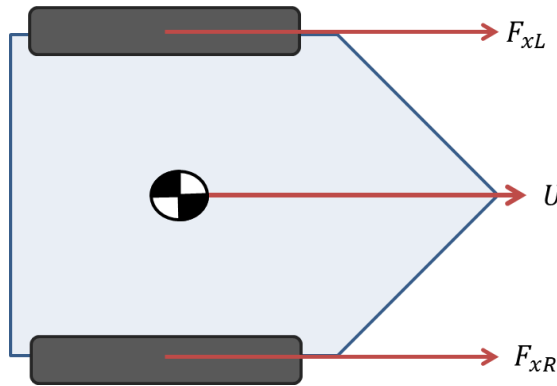

Figure 4. Forces acting on the longitudinal axis of EPW

During descending on the slope, the slip ratio which is the difference in speed between the wheel and EPW must be analyzed to determine whether the EPW is skidding or not. Equation (8) represents the equation of slip ratio during accelerating and braking.

$$\rho_{accelerating} = \frac{R_t \omega - U}{R_t \omega} \tag{8}$$

$$\rho_{braking} = \frac{U - R_t \omega}{U}$$

The friction coefficient, μ on the contact patch between the tire and the road is also affected by the slip ratio. Equation (9) expresses the relation between the slip ratio and the friction coefficient, denoted as μ-ρ function, representing the influence of the road condition parameter. This equation elucidates how the two are interrelated for a given road surface, where k is the parameter of the road surface.

$$\mu_{acc} = 1.05k\{e^{-45\rho} - e^{-0.45\rho}\} \tag{9}$$

$$\mu_{brk} = -1.15k\{e^{-35\rho} - e^{-0.35\rho}\}$$

where,

$$k_{dry\ mosaic} = 0.6$$

$$k_{wet\ mosaic} = 0.12$$

The function of Equation (9) can be illustrated in Figure 5. Based on Figure 5, the optimum slip ratio can be determined to control the wheel from lock-up while descending on the slope.
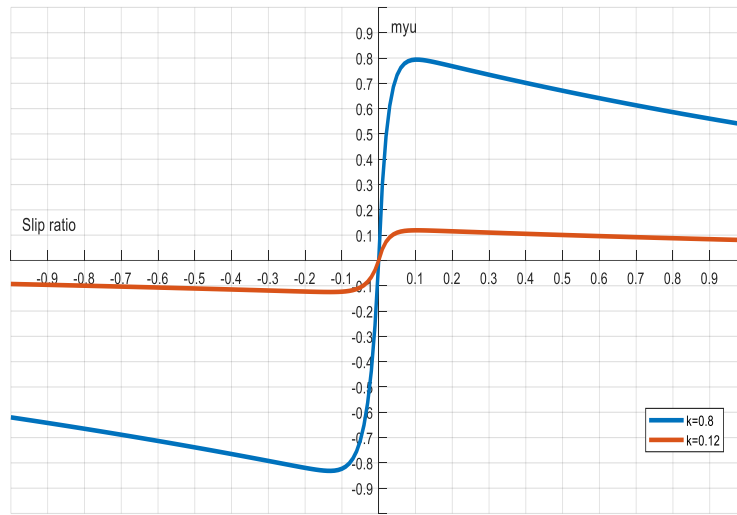
Figure 5. Curve of the relationship between friction coefficient and slip ratio

After calculating the friction of friction, μ, the friction force at each wheel, F_x can be determined as in Equation (10), where F_z is the normal force reaction on the tire.

$$F_x = \mu(\rho) \times F_z \tag{10}$$

2.4   Hill Descent Control (HDC) for EPW

Figure 6 shows the block diagram of EPW that is represented in the state-space equation. This block diagram is designed based on Equation 4 and Equation 5 which have been transformed into the state-space equations as follows:

$$\dot{x} = Ax + Bu \tag{11}$$

$$y_1 = C_1 x = I \tag{12}$$

$$y_2 = C_2 x = \omega \tag{13}$$

where,

$$C_1 = \begin{bmatrix} 1 & 0 \end{bmatrix}$$

$$C_2 = \begin{bmatrix} 0 & 1 \end{bmatrix}$$

$$A = \begin{bmatrix} -\dfrac{R}{L} & -\dfrac{K_t}{L} \\ \dfrac{K_t}{J} & -\dfrac{B}{J} \end{bmatrix}$$

$$x = \begin{bmatrix} I & \omega \end{bmatrix}^T$$

$$B = \begin{bmatrix} \dfrac{1}{L} & 0 \\ 0 & \dfrac{1}{J} \end{bmatrix}$$

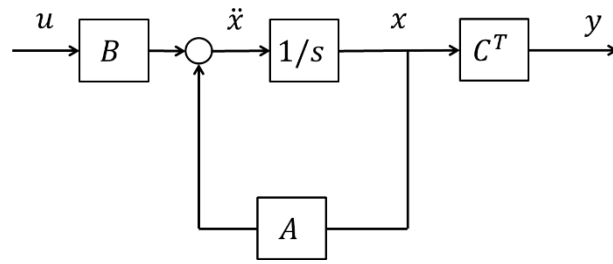$$u = \begin{bmatrix} v & (T_g - T_L - T_f) \end{bmatrix}^T$$

Figure 6. Block diagram of EPW represents in state space equation

Based on the block diagram in Figure 7, the input, u of the plant model is the voltage, V. Therefore, to regulate the speed of the EPW, plugging braking will be employed to provide voltage in the reverse direction, taking into account the back-EMF generated by the BLDC motor. The HDC consists of the controller to minimize and eliminate the error between the desired speed, y_{2d} and the actual speed, y_2. The PID control is used as a control strategy to provide the input, u to the plant model as shown in Figure 8(a). The PID gain is tuned by using the empirical method based on the response shown in Figure 8(b), which is the overshoot and settling time must be less than 5% and 3s respectively, while the steady-state error (SSE) must be ±0.05 [21].
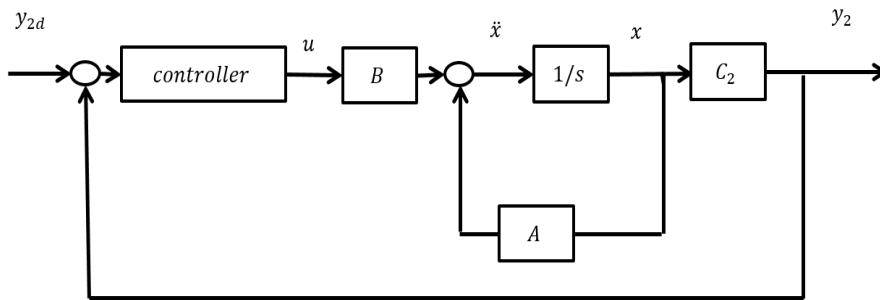

Figure 7. Block diagram of EPW with feedback controller
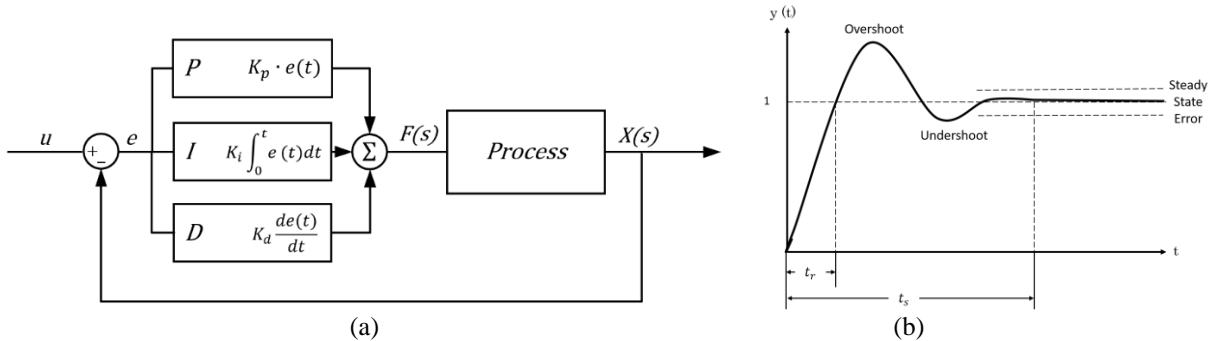

(a)   (b)

Figure 8. (a) Block diagram of PID controller (b) response graph of PID controller

To determine the effectiveness of the plugging brake system with HDC, the simulation is performed when EPW is descending on the slope. In Figure 9, the simulation parameters are depicted. Initially, the EPW initiates movement on a level, dry mosaic surface at a constant speed of 2.5 m/s when the slope angle is 0 degrees. After some time, the EPW transitions to a descent on an 8.1-degree slope. Simultaneously, the plugging brake system featuring HDC is engaged to ensure that the EPW's speed remains consistent with the desired speed of 0.6 m/s until it reaches the end of the slope.
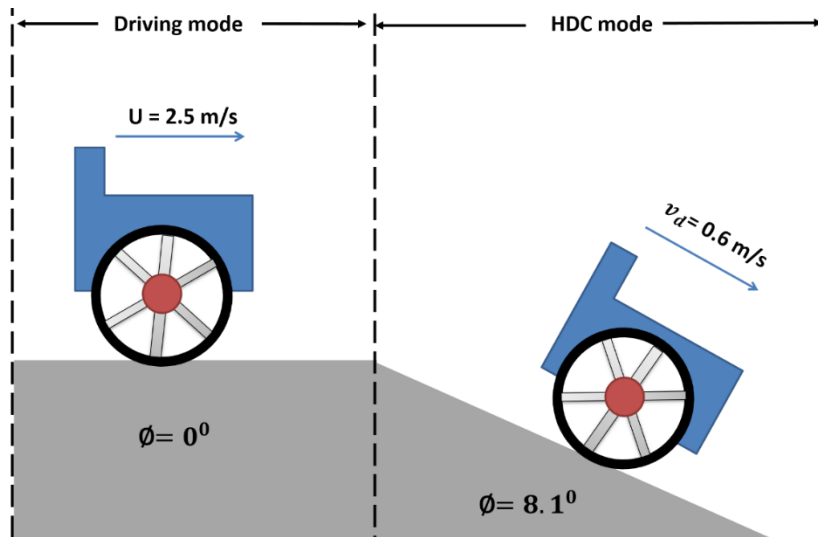
Figure 9. Simulation condition for activating the plugging brake system with HDC

3.0 RESULTS AND DISCUSSIONS

Figure 10 shows the simulation result of the traveled distance starting from driving to the braking mode when the acceleration body, $\dot{U}_x$ in Eq.7, is integrated in a second order to form the travel distance, x. From the result, the EPW took 5 s to travel in 12.4 m in driving mode before changing to braking mode. Next, when the EPW started to apply the plugging braking with HDC, the distance traveled by EPW was increased to 18.2 m in 7.4 s. The slope of the graph before braking is applied steeper than after braking is applied. These two situations show the speed of EPW is changing and slowly decreases when entering different slopes.
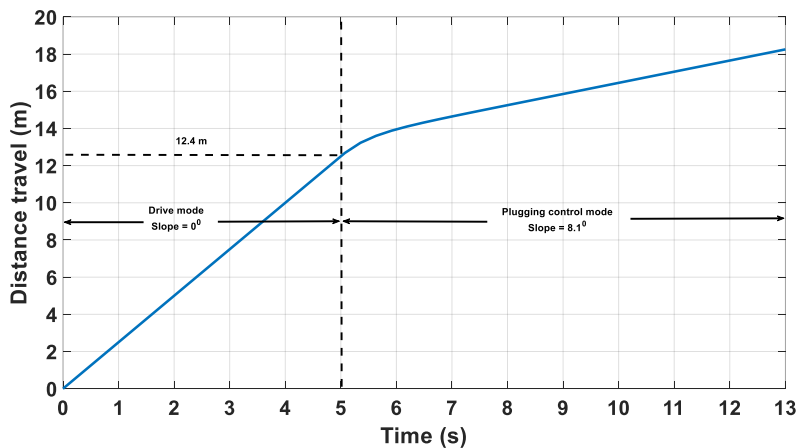

Figure 10. Travelled distance of EPW during driving and braking mode

The effectiveness of the plugging braking with HDC can be seen from the EPW and tire speed, as shown in Figure 11. In the simulation, the desired speed of the EPW and tire is set at 0.6 m/s, which means that when the plugging braking with HDC is activated, both EPW and tire must maintain the speed at 0.6 m/s. In driving mode, both tire and EPW have the same speed at 2.5m/s. When EPW starts descending on the slope, the plugging braking with HDC is activated, and it takes 2.2 s for both EPW and tire to reach 0.6 m/s. Due to the large plugging braking voltage at the initial, the tire gradually decreased than the EPW speed. From the equation of slip ratio (Eq.8) and (Eq.9), when the surface coefficient is set to 0.6 for the dry mosaic surface, the tire is slightly slipping in 0.45 seconds. However, EPW and tire can be maintained at 0.6 m/s after a second. This result shows the plugging braking with the HDC controller gives an effective significant result for EPW when braking at the mosaic surface. Thus, it will increase the safety of EPW when braking on slippery surfaces while maintaining the speed during descending slope conditions.
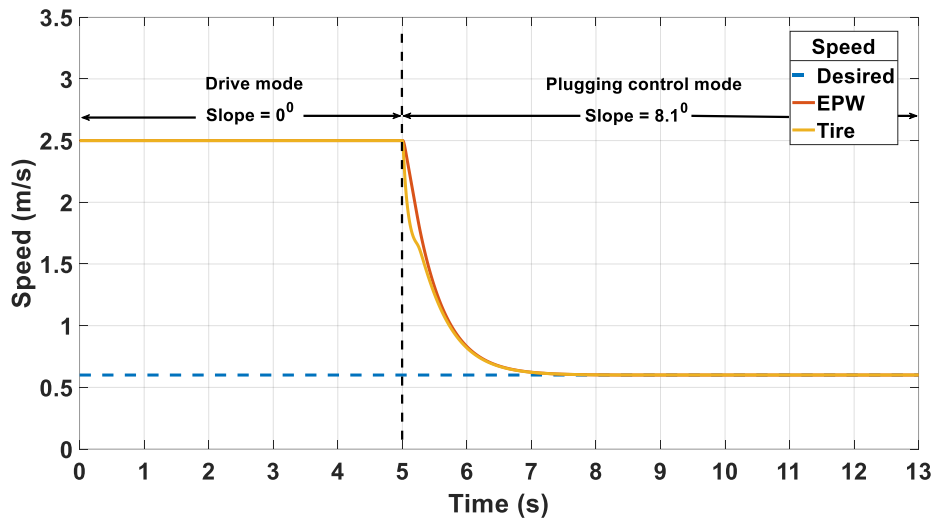
Figure 11. Speed of EPW and tire

The amount of input voltage from the battery for driving mode and the plugging voltage during braking can be seen in Figure 12. In driving mode, to drive an EPW at 2.5 m/s, a 24V input from the battery was applied to the BLDC motor. The plugging brake system is activated when the EPW enters a sloped region. Based on equation (6), when the inverse voltage from plugging is supplied to the motor, the current also becomes inverse. Thus, the torque braking, T_b are produced. Due to the high speed at initial plugging braking activation, the plugging voltage is recorded at -2.8V. However, the plugging voltage decreased gradually and remained constant at -0.49V. This result shows that the amount of plugging voltage to control the speed of the EPW is not too large and acceptable. This can also prevent the BLDC motor from being broken if too large a plugging voltage is required for braking with HDC.
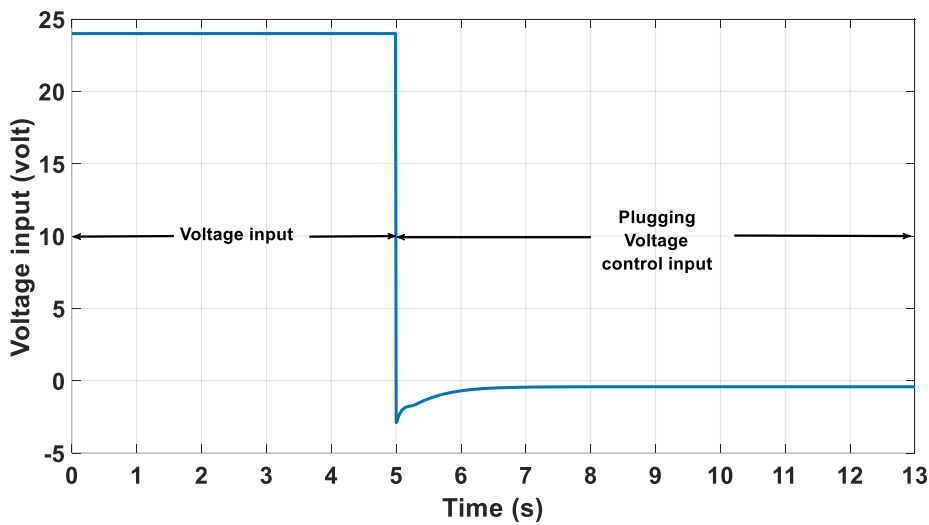

Figure 12. Voltage input during driving and plugging braking mode

Figure 13 shows the analysis of amplitude, steady-state error, and overshoot for analyzing the PID response according to the empirical method with values P, I, and D set to 8.5, 0.07 and 0.3 respectively. As shown in Figure 13, when plugging braking with HDC is activated, the amplitude response plot shows the overshoot is less than 5 % with the amount of 2.45 %. Moreover, the settling time for the EPW and tire start to maintain at the desired speed is 2.3s which is under the required settling time. Furthermore, the plot demonstrates that the amplitude response falls within the desired steady-state error range of ±0.05. This amplitude response graph supports the conclusion that the PID controller is well-suited for the HDC application involving plugging braking.
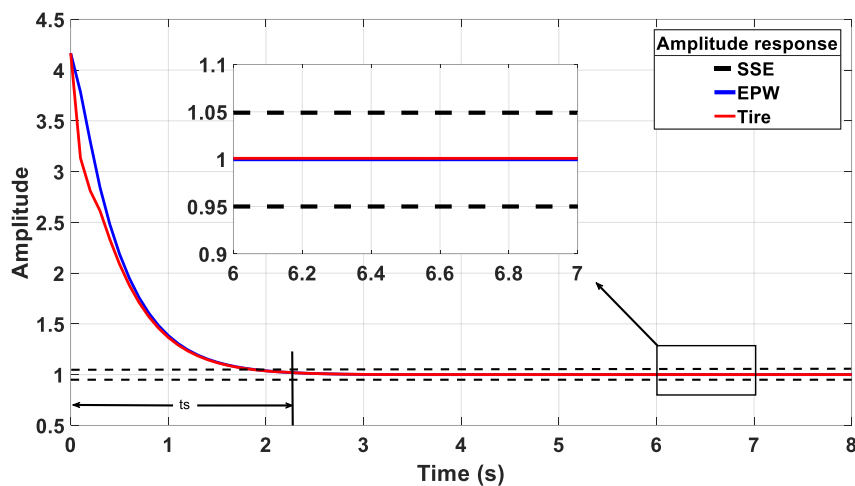
Figure 13. Amplitude response of the speed when HDC with plugging braking is activated

4.0   CONCLUSIONS

In this research, a plugging braking system integrated with HDC using Matlab Simulink to enhance the braking performance of the EPW during downhill descents has been developed. The simulation outcomes demonstrate that when the EPW is moving at a velocity of 2.5 m/s, the plugging braking system with HDC can apply the necessary braking force to reduce the EPW's and the tires' speed to the desired level of 0.6 m/s.

Initially, due to the elevated plugging voltage when plugging braking and HDC are activated, the tires' speed decreases more rapidly than that of the EPW. However, once the EPW and tires reach the desired speed of 0.6 m/s, it can consistently maintain this speed. Empirical methods were employed in the PID control, and the results demonstrate that the settling time and steady-state error fall within the required range. These findings confirm that the proposed approach, employing a plugging braking system with HDC, can enhance the safety of the EPW system.

5.0   ACKNOWLEDGEMENT

6.0   REFERENCES

[1]   M. Pita, "Design and manufacture of solar-Powered wheelchair," *International Journal of Engineering Research & Technology*, vol. 13, no. 9, pp. 2153–2156, 2020.

[2]   T. A. Zarma, A. A. Galadima, and A. A. Maruf, "Review of motors for electric vehicles," *Journal of Scientific Research and Reports*, vol. 24, no. 6, pp. 1–6, 2019.

[3]   B. Wieczorek, "Case study: Influence of the mechanical and electrical anti-rollback system for wheelchair when climbing a hill," *MATEC Web of Conferences*, vol. 357, pp. 1–10, 2022.

[4]   N. A. M. Rusly and S. N. Kamaruzzaman, "Post occupancy evaluation towards facilities improvement for students with disabilities in University of Malaya," *Journal of Building Performance,* vol. 9, no. 2, pp. 1–10, 2018.

[5]   J. Sedlak, R. Vanek, and J. Chladil, "Production of assistance brake for mechanical wheelchair," *Manufacturing Technology*, vol. 18, no. 3, pp. 487–492, 2018.

[6]   I. M. Zulhilmi, P. M. Heerwan, R. I. M. Eiman, I. M. Izhar, and S. M. Asyraf, "Investigation on vehicle dynamic behaviour during emergency braking at different speed," *International Journal of Automotive and Mechanical Engineering*, vol. 16, no. 1, pp. 6161–6172, 2019.

[7]   T. D. Garner and M. D. Ricard, "Effects of trunk functional capacity on the control of angular momentum during manual wheelchair braking," *Open Sports Sciences Journal*, vol. 15, no. 1, pp. 1–8, 2022.

[8]   S. S. Bhurse and A. A. Bhole, "A review of regenerative braking in electric vehicles," *7th IEEE International Conference on Computation of Power, Energy, Information and Communication, ICCPEIC 2018*, pp. 363–367, 2018.

[9]   S. Ramaswami and R. Sundar, "Researchon regenerative and dynamic braking performance in motor application," *International Journal of Innovative Technology and Exploring Engineering*, vol. 8, no. 6 Special Issue 4, pp. 427–430, 2019.

[10]   A. J. Godfrey and V. Sankaranarayanan, "A new electric braking system with energy regeneration for a BLDC motor driven electric vehicle," *Engineering Science and Technology, an International Journal*, vol. 21, no. 4, pp. 704–713, 2018.

[11]   A. Tomporowski and M. Opielak, "Variable-speed drive with series-excited motors in dynamic braking mode," *Eksploatacja i Niezawodność – Maintenance and Reliability*, vol. 14, no. 3, pp. 222–227, 2012.

[12]   S. M. Asyrafs, P. M. Heerwan, I. M. Izhar, I. M. Zulhilmi, and I. M. Sollehudin, "Comparison of braking performance between mechanical and dynamic braking for Electric Powered Wheelchair," *IOP Conference Series: Materials Science and Engineering*, vol. 469, no. 1, 2019.

[13]   A. T. Hamada and M. F. Orhan, "An overview of regenerative braking systems," *Journal of Energy Storage*, vol. 52, no. 105033, 2022.

[14]   J. Manikandan and M. Arun, "A review on regenerative braking methodology in electric vehicle," *International Journal of Psychosocial Rehabilitation*, vol. 23, no. 4, pp. 220–226, 2019.

[15]   B. Saha and B. Singh, "An economical approach for solar PV-Battery based e-rickshaw with regenerative braking using sensorless BLDC motor drive," *9th IEEE International Conference Power Electronics, Drives and Energy Systems (PEDES)*, pp. 809–814, 2020.

[16]   S. Mehta and S. Hemamalini, "A dual control regenerative braking strategy for two-wheeler application," *Energy Procedia*, vol. 117, no. August 2011, pp. 299–305, 2017.

[17]   W. Li, H. Du, and W. Li, "Driver intention based coordinate control of regenerative and plugging braking for electric vehicles with in-wheel PMSMs," *IET Intelligent Transport Systems*, vol. 12, no. 10, pp. 1300–1311, 2018.

[18]   N. R. Somrajan and P. K. Sreekanth, "Plugging braking for electric vehicles powered by DC Motor," *International Journal of Modern Trends in Engineering & Research*, vol. 3, no. 1, pp. 352–356, 2016.

[19]   L. Sun and B. Xu, "An improved method for discerning broken rotor bar fault and load oscillation in induction motors," *Energies*, vol. 11, no. 11, p. 3130, 2018.

[20]   H. Seki, K. Ishihara, and S. Tadakuma, "Novel regenerative braking control of electric power -assisted wheelchair for safety downhill road driving," *2009 2nd IEEE/RAS-EMBS International Conference on Biomedical Robotics and Biomechatronics*, vol. 56, no. 5, pp. 143–148, 2009.

[21]   M. A. M. Dzahir *et al.*, "Optimal tuning of a pid controller for emdap- cvt using particle swarm optimization," *Jurnal Teknologi Full paper*, vol. 11, pp. 135–141, 2015.